Xenon low-n Rydberg states in supercritical argon near the critical point

Luxi Li [a,b], Xianbo Shi [a,b], C.M. Evans [a,b,*], G.L. Findley [c]

[a] *Department of Chemistry and Biochemistry, Queens College – CUNY, Flushing, NY 11367, United States*

[b] *Department of Chemistry, Graduate Center – CUNY, New York, NY 10016, United States*

[c] *Department of Chemistry, University of Louisiana at Monroe, Monroe, LA 71209, United States*

Abstract

We present vacuum ultraviolet absorption spectra and an asymmetric line shape simulation of the $6s$ and $6s'$ Rydberg states (including the blue satellite bands) of xenon doped into argon, from low argon number density to the density of the triple point liquid, at both noncritical temperatures and near (+0.5°C) the critical isotherm of argon (i.e., −122.3°C). The argon induced shift in the simulated primary transition of the Xe $6s$ and $6s'$ Rydberg states is presented as a function of argon number density for noncritical temperatures and along an isotherm near the critical temperature. This shift demonstrates a perturber critical point effect on the transition energies of low-n dopant Rydberg states.

* Corresponding author.
Email address: cherice.evans@qc.cuny.edu (C.M. Evans).

1 Introduction

The structure of dopant electronic states in dense perturbing fluids is very important in understanding solvent effects in photochemical reactions. Recent studies have shown that dopant vibrational frequencies [1] and ionization energies [2] exhibit dramatic changes near the critical temperature and density of the perturber. Although critical point effects have also been observed in the perturber induced energy shift of dopant valence transitions [1], these low energy electronic states are not the best probes for such studies, since they are relatively insensitive to the perturber environment [3]. At the other extreme, high-n Rydberg states are very perturber sensitive due to their large 'orbital' nature; however, they are closely spaced energetically and, therefore, cannot be resolved as the perturber number density increases. Low-n Rydberg states, on the other hand, are energetically isolated while retaining the environmental sensitivity that is characteristic of all Rydberg states [3], thus ensuring that the perturber induced line shape broadening and energy shift can be modeled for a large number of perturber densities. These states, then, are excellent probes to investigate perturber effects on excited electronic states.

The Xe $6s$ and $6s'$ Rydberg state absorption spectra are well characterized [4–8] and have been shown to shift and broaden significantly as a function of perturber number density [4,5]. Messing *et al.* [4,5] were the first to investigate the broadening and shift of the Xe low-n Rydberg states doped into argon. These authors [4,5] used a standard moment analysis to extract the perturber dependent shift $\Delta(\rho_{\mathrm{Ar}})$ [where ρ_{Ar} is the argon number density] of the Xe $6s$ and $6s'$ Rydberg states, and they showed that $\Delta(\rho_{\mathrm{Ar}})$ tends first to lower energy and then to higher energy as ρ_{Ar} increases from low density to the density of

the triple point liquid. However, since Messing *et al.* did not explore critical temperature effects on $\Delta(\rho_{\rm Ar})$, they concluded that perturber effects on dopant Rydberg states are independent of temperature [4,5]. Moreover, their moment analysis [4,5] did not correctly account for the appearance and growth of the blue satellite bands on the shoulder of the primary Rydberg transition. These satellite bands, which are shown in Fig. 1 and which have been identified with the formation of ground and excited state XeAr dimers [6–8], increase in intensity and broaden as a function of argon density. In fact, these bands grow to the point that the primary Xe Rydberg transition can no longer be distinguished from the broad blue satellite bands. Thus, the moment analysis performed by Messing *et al.* [4,5] yielded incorrect energies for the primary transitions. This incorrect moment analysis, coupled with the asymmetric line broadening, led to difficulties in modeling $\Delta(\rho_{\rm Ar})$ [4,5] within the semi-classical statistical theory for line shape analysis [9]. Messing *et al.* [4,5] overcame these difficulties by using different sets of intermolecular potential parameters for different perturber number densities.

In this paper, we present new absorption measurements and a full simulation of the $6s$ and $6s'$ Rydberg states of xenon doped into argon, from low argon number density to the density of the triple point liquid, at both noncritical temperatures and near ($+0.5$°C) the critical isotherm of argon (i.e., -122.3°C). Our simulation uses a single set of intermolecular potential parameters for the entire density range, and in order to accurately model the line shape, we have included the primary transition

$$\mathrm{Xe} + h\nu \quad \xrightarrow{\mathrm{Ar}} \quad \mathrm{Xe}^* \,, \tag{1}$$

denoted a in Fig. 1, as well as the XeAr dimer transitions that yield the blue satellite bands, namely [6–8]

$$\mathrm{XeAr} + h\nu \quad \xrightarrow{\mathrm{Ar}} \quad \mathrm{Xe}^* + \mathrm{Ar}\ , \tag{2}$$

and

$$\mathrm{XeAr} + h\nu \quad \xrightarrow{\mathrm{Ar}} \quad \mathrm{Xe}^*\mathrm{Ar}\ , \tag{3}$$

denoted b and c, respectively in Fig. 1. A moment analysis on the simulated primary transition [i.e., eq. (1), a in Fig. 1] is then used to study the perturber critical point effect on dopant electronic states. We thereby show that the perturber induced shift of the first moment of the primary transition for both the $6s$ and $6s'$ Rydberg states increases near the critical density and temperature, which is similar to the behavior seen in vibrational bands and valence transitions [1].

2 Experiment

The experimental details have been given previously [10]. Briefly, photoabsorption spectra were measured with monochromatized synchrotron radiation having a resolution of $\sim$ 8 meV in the spectral region of interest. This radiation entered a copper experimental cell, equipped with entrance and exit MgF_2 windows (with an energy cut-off of 10.9 eV), that is capable of withstanding pressures of up to 100 bar. The cell was connected to an open flow liquid nitrogen cryostat and resistive heater system that allowed the temperature to be controlled to within $\pm$ 0.5°C at non-critical temperatures and to within $\pm$ 0.2°C at a temperature near the critical isotherm. To prevent liquid formation in the cell during temperature stabilization, the set point for the

critical isotherm was chosen to be −121.8°C, which is near the argon critical temperature of −122.3°C. The pathlength of the cell is 1.0 cm. All transmission spectra were normalized both to the incident light intensity and to the empty cell transmission. Once corrected, the transmission spectra were converted to absorbance and normalized to one, in order to allow for comparison with the simulated line shapes. Xenon (Matheson Gas Products, 99.995%) and argon (Matheson Gas Products, 99.999%) were used without further purification. The absence of trace impurities in the spectral range of interest was verified by the measurement of photoabsorption spectra for xenon and argon. The number density of argon was calculated from the Strobridge equation of state [11], using a standard iterative technique. The xenon concentration was optimized for each argon number density, but never exceeded 10 ppm. Both the gas handling system and the procedures used to ensure homogeneous mixing of the dopant and perturber have been described previously [10]. Prior to the introduction of xenon, the experimental cell and gas handling system were baked to a base pressure of 10^{-8} Torr. In order to ensure no xenon contamination of argon, the gas handling system was allowed to return to the low 10^{-7} Torr range after the addition of xenon but before the addition of argon.

Since the satellite bands shown in Fig. 1 become more intense as ρ_{Ar} increases, they must be accurately simulated along with the primary transitions in order to reproduce the experimental line shape at medium to high ρ_{Ar}. The intermolecular potentials employed and the methods used to simulate these line shapes are discussed in more detail below.

3 Results and Discussion

Within a semi-classical approximation, the spectral line shape can be written as a Fourier transform, namely [4,5,12]

$$\mathfrak{L}(\omega) = \frac{1}{2\pi}\,\mathrm{Re}\int_{-\infty}^{\infty} dt\ \mathrm{e}^{-i\omega t}\langle \mathrm{e}^{i\omega(\mathbf{R})t}\rangle\ , \tag{4}$$

where $\langle\cdots\rangle$ represents the thermal average, $\mathbf{R}$ denotes the collection of all dopant/perturber distances, and $\omega = \omega(\mathbf{R}) - \omega_0$, with ω_0 being the transition frequency for the neat dopant. Eq. (4) neglects lifetime broadening and assumes that the transition dipole moment is independent of $\mathbf{R}$. Substituting an exponential density expansion for the thermal average in eq. (4) yields [4,5,12]

$$\mathfrak{L}(\omega) = \frac{1}{2\pi}\,\mathrm{Re}\int_{-\infty}^{\infty} dt\ \mathrm{e}^{-i\omega t}\ e^{A_1(t)+A_2(t)+\cdots}\quad , \tag{5}$$

where $A_1(t)$ is

$$A_1(t) = 4\pi\rho_{\mathrm{P}}\int_0^{\infty} dr\ r^2\ g_{\mathrm{PD}}(r)\left[\ e^{-it\Delta V(r)} - 1\ \right]\quad , \tag{6}$$

and $A_2(t)$, within the Kirkwood superposition approximation, is given by

$$\begin{aligned} A_2(t) = \ & 4\pi\rho_{\mathrm{P}}^2\int_0^{\infty} dr_1\ r_1^2\ g_{\mathrm{PD}}(r_1)\ \left[e^{-it\Delta V(r_1)} - 1\right] \\ & \times\int_0^{\infty} dr_2\ r_2^2\ g_{\mathrm{PD}}(r_2)\ \left[\ e^{-it\Delta V(r_2)} - 1\ \right] \\ & \times\frac{1}{r_1\ r_2}\ \int_{|r_1-r_2|}^{|r_1+r_2|} s\ [\ g_{\mathrm{PP}}(s) - 1\ ]\ ds\ . \end{aligned} \tag{7}$$

In eqs. (5) - (7), $g_{\mathrm{PD}}(r)$ is the ground state perturber/dopant radial distribution function, $g_{\mathrm{PP}}(r)$ is the perturber/perturber radial distribution function, ρ_{P} is the bulk density of perturber, and $\Delta V(r) = V_e(r) - V_g(r)$, where $V_e(r)$ and $V_g(r)$ are, respectively, the excited and ground state dopant/perturber intermolecular potentials. $A_1(t)$ represents the average two-body dopant/perturber interactions, while $A_2(t)$ is an approximation to the three body interactions

in the system. Since higher order interactions are more difficult to model, and since the strength of the interaction decreases as the number of bodies involved increases, our line shape simulations truncated the exponential density expansion at $A_2(t)$.

The required radial distribution functions were obtained from a coupled integro-differential equation method [13], while the Fourier transform of eq. (5) was performed using a standard fast Fourier transform algorithm [14]. All calculations were performed with a step size of 6.818×10^{-2} Å for the radial distribution functions and a time step of 2.068×10^{-15} s for the fast Fourier transform. The line shape obtained from the transform of eq. (5) was convoluted with a standard Gaussian slit function to account for the finite ($\sim$ 8 meV) resolution of the monochromator.

A standard Lennard-Jones 6-12 potential

$$V(r) \;=\; 4\,\varepsilon \left[\left(\frac{\sigma}{r}\right)^{12} \;-\; \left(\frac{\sigma}{r}\right)^{6} \right] \tag{8}$$

was chosen for all of the ground state intermolecular interactions (i.e., Ar/Ar, Xe/Ar, and XeAr dimer/Ar), while all excited state intermolecular interactions were modeled using an exponential-6 potential

$$V(r) \;=\; \frac{\varepsilon}{1-(6/\gamma)} \left\{ \frac{6}{\gamma}\, e^{\gamma(1-\chi)} - \left(\frac{1}{\chi}\right)^{6} \right\} . \tag{9}$$

In eqs. (8) and (9), ε is the well-depth, σ is the collision parameter, $\chi \equiv r/r_e$ (where r_e is the equilibrium distance), and γ is the potential steepness. All intermolecular potential parameters except the Ar/Ar ground state intermolecular potential were adjusted to give the best simulated line shape in comparison to experiment. The values for all parameters used are given in Table 1. The relative intensities of the simulated bands were set by comparison to the

photoabsorption spectra of Xe doped into argon at a number density of argon where all bands could be clearly identified. Experimentally, at low argon number densities the ratio of heights between the b band and the primary transition is 0.2 for both the Xe $6s$ and $6s'$ Rydberg states in Ar. For the Xe $6s$ Rydberg state in Ar, the ratio of heights between the c band and the primary transition is 0.45.

Figs. 2 and 3 compare the experimental photoabsorption spectra with the simulated line shapes for the Xe $6s$ and $6s'$ transitions at noncritical temperatures (Fig. 2) and on an isotherm near the critical temperature (Fig. 3). Clearly, the simulated spectra closely match the measured spectra for all densities. Both the simulated and experimental line shapes show a slight shift to lower energies at low argon number densities, followed by a strong shift to higher energies at high argon number densities, similar to the original observations of Messing *et al.* [4,5]. The ground state interaction between Xe and Ar (or XeAr and Ar) is attractive and, therefore, the ground states are stabilized by the argon solvent shell. The slight red shift observed at low argon number densities indicates that the xenon excited states (either Xe* or Xe*Ar) are also stabilized by the argon solvent shell. As the density increases, however, argon begins to shield the optical electron from the xenon cationic core, thereby decreasing the binding energy of the optical electron. Thus, as the density of argon increases the energy of the excited state also increases, leading to a blue shift in the transition energy at higher perturber densities and near the critical point of the perturber.

With an accurate simulation of the primary transition for both the Xe $6s$ and $6s'$ Rydberg states in argon, a line shape analysis was performed to determine the argon induced shift $\Delta(\rho_{\mathrm{Ar}})$ of the primary transition. $\Delta(\rho_{\mathrm{Ar}})$ was

approximated as the first moment [5]

$$M_1 = \int \mathfrak{L}(E)\, E\, dE \Big/ \int \mathfrak{L}(E)\, dE \quad , \tag{10}$$

where $\mathfrak{L}(E)$ is the simulated absorption band for the primary transition and $E = \hbar(\omega - \omega_0)$ ($\hbar \equiv$ reduced Planck constant). As shown in Fig. 4, even though the peak of the primary transition red shifts at very low argon densities, the first moment of the band does not because the line shape is blue degraded. Moreover, a distinct critical point effect of the order of 20 meV is observed. This effect results from an increase at the critical point of the perturber number density near a dopant atom, as reflected in the radial distribution functions that underlie the simulations presented in Figs. 2 and 3. (A similar effect has been predicted by Larrégaray *et al.* [15] for the A $^2\Sigma^+(3s\sigma)$ Rydberg state of nitric oxide in argon, based upon molecular dynamics calculations.)

In this paper, we have shown that the absorption line shapes of low-n atomic Rydberg transitions doped into an atomic perturber can be accurately simulated across a broad perturber density range with an appropriate choice of one set of intermolecular potentials and potential parameters. A general understanding of the density dependence of these line shapes was developed, and a critical point effect was observed in the argon-induced shift $\Delta(\rho_{\mathrm{Ar}})$ of the simulated primary transition for the low-n Xe Rydberg states.

Acknowledgements

We thank Dr. Seogjoo Jang (Queens College – CUNY) for many helpful discussions in programming the fast Fourier transforms. All experimental measurements were made at the University of Wisconsin Synchrotron Radiation

Center (NSF DMR-0537588), with support from the Petroleum Research Fund (PRF#5-24880), the Professional Staff Congress - City University of New York and the Louisiana Board of Regents Support Fund (LEQSF(2006-09)-RD-A-33).

References

[1] S. C. Tucker, Chem. Rev. 99 (1999) 391, and references therein.

[2] Xianbo Shi, Luxi Li, C. M. Evans, G. L. Findley, Nucl. Inst. Meth. A 582 (2007) 270, and references therein.

[3] M. B. Robin, Higher Excited States of Polyatomic Moleculeles Vol.I-Vol.III, Academic Press, 1974, 1975, 1985, and references therein.

[4] I. Messing, B. Raz, J. Jortner, J. Chem. Phys. 66 (1977) 2239.

[5] I. Messing, B. Raz, J. Jortner, J. Chem. Phys. 66 (1977) 4577.

[6] R. Granier, M. C. Castex, J. Granier, J. Romand, C. R. Acad. Sci. Ser. B 264 (1967) 778.

[7] M. C. Castex, R. Granier, J. Romand, C. R. Acad. Sci. Ser. B 268 (1969) 552.

[8] M. C. Castex, J. Chem. Phys. 66 (1977) 3854.

[9] R. Kubo, and Y. Toyozawa, Prog. Theoret. Phys. Japan 13 (1955) 160.

[10] C. M. Evans. Ph.D Dissertation, Louisiana State University, Baton Rouge, LA, 2001; see also C. M. Evans, J. D. Scott, G. L. Findley, Rec. Res. Chem. Phys. 3 (2002) 351.

[11] A. L. Gosman, R. D. McCarty, J. G. Hust, NSRDS-NBS (1969) 27.

[12] S. A. Egorov, M. D. Stephens, J. L. Skinner, J. Chem. Phys. 107 (1997) 10485.

[13] E. W. Grundke, D. Henderson, R. D. Murphy, Can. J. Phys. 51 (1973) 1216.

[14] W. H. Press, S. A. Teukolsky, W. T. Vetterling, B. P. Flannery, Numerical Recipes in FORTRAN: the art of scientific computing, Cambridge University Press, New York, 1992.

[15] P. Larrégaray, A. Cavina, M. Chergui, Chem. Phys. 308 (2005) 13.

Table 1
Intermolecular potential parameters for eqs. (8) and (9).

	$\varepsilon/k_{\mathrm{B}}$ (K)	r_e (Å)	γ
Ar/Ar[a]	119.5	3.826[b]	–
Xe/Ar	147.9	4.213[b]	–
XeAr/Ar	146.0	4.265[b]	–
Xe $6s$/Ar	200.0	5.370	14.75
Xe $6s'$/Ar	215.0	5.400	14.75
Xe($6s$)Ar/Ar	300.0	5.075	14.75

[a]Parameters obtained from Ref. [2].
[b]For a Lennard-Jones 6-12 potential, $\sigma = 2^{-1/6} r_e$.

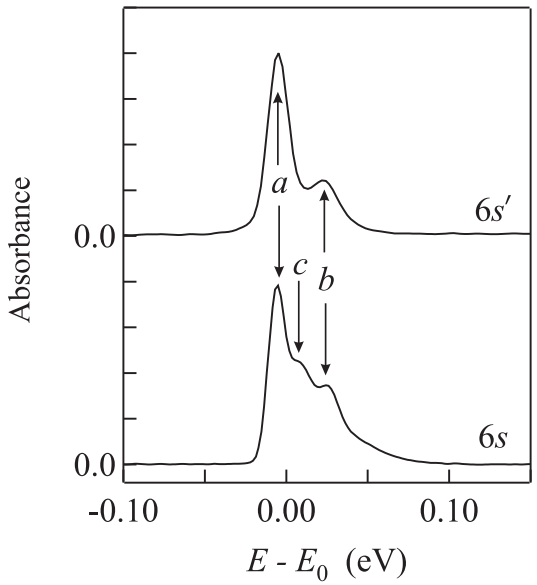

Fig. 1. Experimental absorbance (relative scale) of Xe $6s$ and $6s'$ doped into Ar at an argon number density of $\rho_{\mathrm{Ar}} = 1.47 \times 10^{21}$ cm^{-3} at room temperature (23.6°C). a corresponds to eq. (1), b to eq. (2), and c to eq. (3). For the $6s$ Rydberg state, $E_0 = 8.437$ eV; for the $6s'$ Rydberg state, $E_0 = 9.570$ eV.

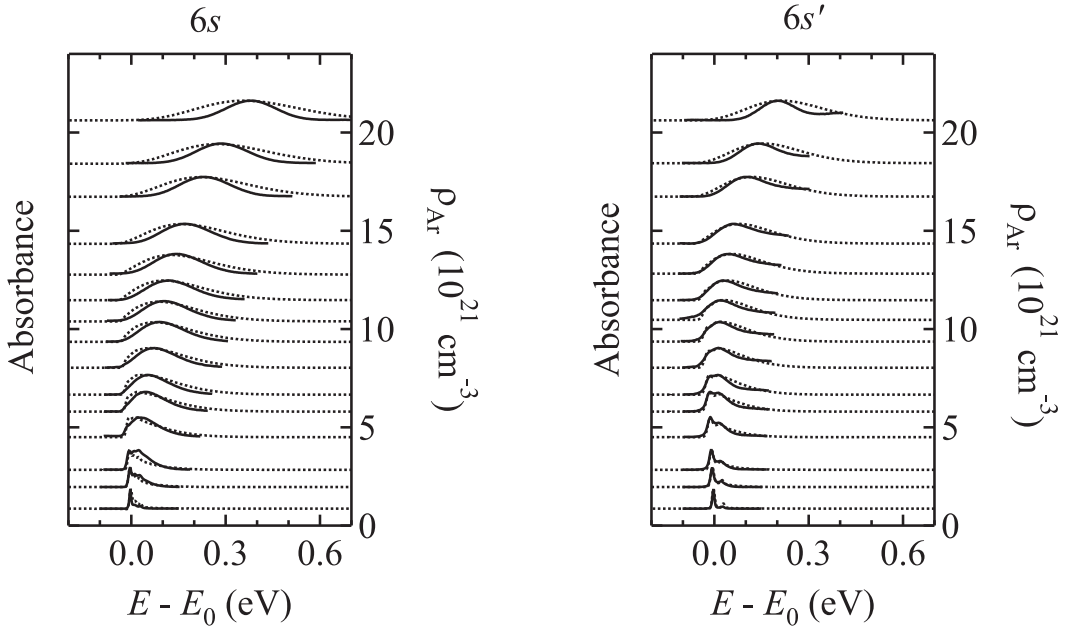

Fig. 2. Selected experimental absorbance (—, relative scale) and simulated line shapes ($\cdots$) for the Xe $6s$ and $6s'$ Rydberg transitions at noncritical temperatures. The data are offset vertically by the argon perturber number density ρ_{Ar}. The energy offsets E_0 are given in Fig. 1.

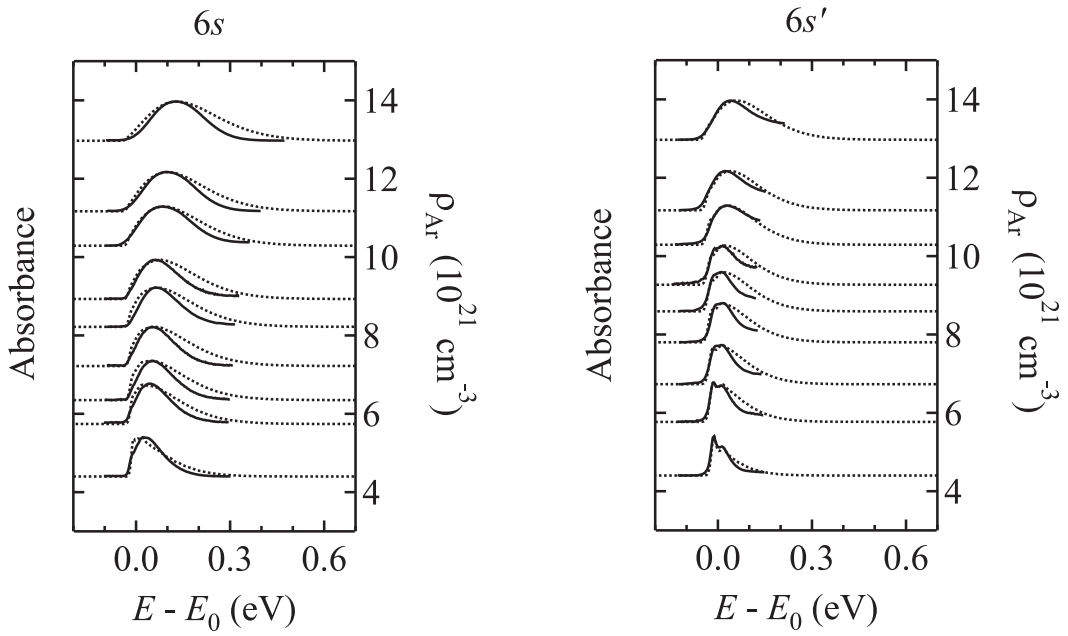

Fig. 3. Selected experimental absorbance (—, relative scale) and simulated line shapes ($\cdots$) for the Xe $6s$ and $6s'$ Rydberg transitions on an isotherm (-121.8°C) near the critical isotherm. The data are offset vertically by the argon perturber number density ρ_{Ar}. The energy offsets E_0 are given in Fig. 1.

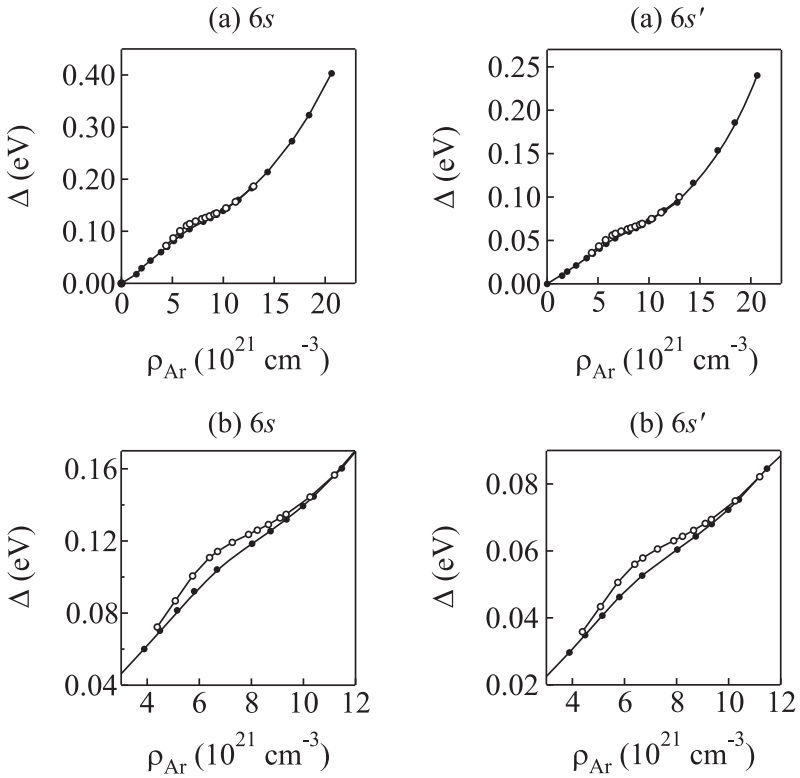

Fig. 4. (a) The argon induced shift Δ, as approximated by eq. (10), of the simulated primary transition for the Xe $6s$ and $6s'$ Rydberg states as a function of argon number density $\rho_{\rm Ar}$ at ($\bullet$) non-critical temperatures and ($\circ$) near the critical isotherm. (b) An expanded view of the region near the argon critical density of 8.0×10^{21} cm^{-3}. The solid lines are a visual aid. See text for discussion.